A Dual-Layer Perturbation-Based Pied Kingfisher Optimizer for Solving the Economic Load Dispatch Problem

Xin-Yi Guan, Jie-Sheng Wang *, Hao-Ming Song, Jia-Hui Zhao

Abstract—**To address the limitations of the Pied Kingfisher Optimizer (PKO), such as premature convergence and limited global search capability when solving complex optimization problems, this paper proposes an improved algorithm based on a dual-disturbance mechanism. The proposed method first incorporates a probabilistically controlled reverse perturbation strategy to enhance population diversity. Subsequently, a dual-disturbance mechanism is constructed by integrating multiple heavy-tailed distributions, including Lévy flight, Cauchy distribution, Student's t-distribution, and Laplace distribution, to strengthen the ability to escape from local optima. The mechanism promotes a more effective trade-off between exploration and exploitation during optimization. Its performance was rigorously evaluated on the CEC-BC-2022 benchmark set. The results demonstrate that the improved algorithm, referred to as LO-PKO, achieves superior optimal values, mean performance, and convergence speed on most test functions, significantly outperforming the original PKO and other enhanced variants. Furthermore, the LO-PKO algorithm was applied to the Economic Load Dispatch (ELD) problem involving both 20 and 40 generating units to further evaluate its scalability and effectiveness in solving large-scale engineering optimization tasks. The experimental results demonstrate that LO-PKO consistently achieves the lowest total generation cost while strictly adhering to all operational constraints in both cases. These findings confirm the algorithm's superior optimization capability, scalability and applicability in addressing complex and real-world power system scheduling problems.**

Index Terms—**Economic Load Dispatch, Pied Kingfisher Optimizer (PKO), Dual-Disturbance Mechanism, Probabilistic Reverse Perturbation, Heavy-Tailed Perturbation**

I. Introduction

With the rapid development of artificial intelligence and computational intelligence, meta-heuristic optimization techniques have emerged as powerful tools for addressing a broad spectrum of complex real-world problems. Among them, swarm intelligence algorithms have garnered increasing attention due to their inherent advantages, including derivative-free search capability, strong global exploration potential, adaptability to various optimization landscapes, and ease of implementation.

These algorithms are inspired by the collective behaviors and self-organizing principles observed in biological populations such as birds, fish, ants, and insects, which exhibit intelligent group behaviors through local interactions and information sharing among individuals.

Unlike gradient-based optimization methods that require continuous and differentiable objective functions, Swarm intelligence algorithms are well-suited for solving non-differentiable, non-convex, multi-modal, and high dimensional problems. Prominent examples include Particle Swarm Optimization (PSO) [1], Grey Wolf Optimizer (GWO) [2] and Differential Evolution (DE) [3], which have been extensively studied and successfully applied in various fields such as numerical optimization, robotics path planning, image analysis, resource scheduling, and power system operations [4].

Swarm intelligence algorithms have been applied to the Economic Load Dispatch (ELD) problem, which minimizes fuel cost subject to operational constraints such as power balance, generation limits, ramp rates, and transmission losses [5]. ELD is challenging due to its nonlinear, non-convex, and multi-constraint nature, especially with valve-point effects and prohibited zones. Traditional deterministic methods often fail to find global optima in such complex scenarios.

In contrast, Swarm intelligence algorithms provide a promising alternative, as they do not rely on gradient information or assumptions about the problem's structure. Their stochastic search mechanisms and population-based exploration facilitate better adaptation to diverse and rugged search landscapes, making them highly effective for solving ELD problems and other real-world engineering challenges [6].

However, despite their advantages, many existing swarm-based optimizer suffer from limitations such as premature convergence, local stagnation and inefficient search dynamics, particularly in high-dimensional and multi-modal problem spaces. To address these challenges, recent studies have introduced stochastic perturbation strategies grounded in heavy-tailed probability distributions, such as Lévy flights

Manuscript received June 4, 2025; revised July 29, 2025. This work was supported by the Basic Scientific Research Project of Institution of Higher Learning of Liaoning Province (Grant No. LJ222410146054), and Postgraduate Education Reform Project of Liaoning Province (Grant No. LNYJG2022137).

Xin-Yi Guan is a postgraduate student at School of Electronic and Information Engineering, University of Science and Technology Liaoning, Anshan, 114051, P. R. China (e-mail: gxy@stu.ustl.edu.cn).

Jie-Sheng Wang is a professor of School of Electronic and Information Engineering, University of Science and Technology Liaoning, Anshan, 114051, P. R. China (Corresponding author, phone: 86-0412-2538246; fax: 86-0412-2538244; e-mail: wjs@ustl.edu.cn).

Hao-Ming Song is a doctoral student of School of Electronic and Information Engineering, University of Science and Technology Liaoning, Anshan, 114051, P. R. China (e-mail: shm@stu.ustl.edu.cn).

Jia-Hui Zhao is a postgraduate student at School of Electronic and Information Engineering, University of Science and Technology Liaoning, Anshan, 114051, P. R. China (e-mail: zjh@stu.ustl.edu.cn).

[7], Cauchy distribution [8], Student's t-distribution [9] and Laplace distribution [10].

These distributions differ from the traditional Gaussian distribution in that they offer a significantly higher likelihood of generating large jump steps, thereby enhancing the global exploration ability of optimization algorithms and improving their capacity to escape local optima. Empirical evidence has demonstrated that integrating heavy-tailed perturbations into meta-heuristic frameworks enhances population diversity, convergence speed, search robustness, and global optimum [11].

Motivated by these insights, this study proposes an enhanced variant of the recently introduced Pied Kingfisher Optimizer (PKO) [12], which is inspired by the predatory diving behavior of pied kingfishers. Although the original PKO has shown promise in global optimization, it suffers from limited exploitation capacity and vulnerability to premature convergence when tackling high-dimensional or rugged landscapes. To overcome these shortcomings, we present a novel dual-disturbance framework, which incorporates two key mechanisms. (1) A probabilistic reverse learning perturbation to diversify the search trajectory. (2) The integration of heavy-tailed distributions to facilitate long-distance exploration.

Based on this framework, five improved PKO variants are developed as O-PKO, LO-PKO (Lévy-based), CO-PKO (Cauchy-based), TO-PKO (Student's t-based) and LAO-PKO (Laplace-based). These variants are systematically evaluated on complex numerical benchmarks to investigate their optimization efficacy and robustness. To validate the proposed algorithms, extensive experiments are conducted on the CEC-BC-2022 benchmark suite, which encompasses a variety of function types including multi-modal, rotated, discontinuous, hybrid and composition functions.

Experimental results reveal that the proposed variants significantly outperform the original PKO across most evaluation criteria. Among them, the LO-PKO algorithm demonstrates the most consistent and superior performance, indicating the effectiveness of Lévy-based perturbation in high-dimensional optimization.

Furthermore, to assess real-world applicability, the best-performing LO-PKO variant is applied to two widely studied ELD test cases involving 20-unit and 40-unit systems [13]. The algorithm's performance is benchmark against the original PKO and several state-of-the-art meta-heuristics, including Newton-Raphson-Based Optimizer (NRBO) [14], Splendid Fairywren Optimization Algorithm (SFOA) [15], Tuna Swarm Optimizer (TSO) [16] and Rapidly-exploring Random Tree-Based Optimizer (RRTO) [17].

Simulation results confirm that LO-PKO achieves the lowest total generation cost while satisfying all system constraints, demonstrating its high potential for practical deployment in large-scale power system optimization.

In summary, this study contributes an advanced PKO framework augmented with stochastic heavy-tailed perturbation strategies, offering enhanced balance between global exploration and local exploitation. The proposed methods exhibit strong performance on both synthetic benchmarks and real-world ELD scenarios, providing new insights into the design of robust and efficient swarm intelligence algorithms for complex optimization problems.

II. Pied Kingfisher Optimizer

A. Initialization

The PKO algorithm starts by randomly initializing a population within the search space, defined as:

$$X_{i,j} = LB + (UB - LB) \times rand\,,$$
$$i = 1,2,\ldots,N \; and \; j = 1,2,\ldots,Dim \quad (1)$$

where, $X_{i,j}$ is the position of the i-th individual in the j-th dimension, $rand$ is a random value in [0,1], and UB and LB are the search space bounds.

B. Perching and Hovering Strategy (Exploration Phase)

During exploration, PKO mimics hovering to update positions:

$$X_i(t+1) = X_i(t) + \alpha \times T \times (X_j(t) - X_i(t)),$$
$$i, j = 1,2,\ldots,N \; and \; j \neq i \quad (2)$$

During iteration, $X_i(t+1)$and $X_i(t)$ represent the current and updated positions, respectively. The parameter α is computed as $2 \times randn(1, Dim) - 1$, where $randn$ follows a standard normal distribution. N and Dim denote the population size and problem dimension, while T is adaptively set based on the current strategy and behavior phase.

When perching, the parameter T is calculated as follows:

$$T = (exp(1) - exp(\frac{t-1}{Max\_Iter})^{\frac{1}{BF}}) \times cos(Crest\_angles) \quad (3)$$

where, Max_Iter is the maximum number of iterations, BF is a constant set to 8, and $rand$ is a uniformly distributed random value in [0, 1].

When hovering, the parameter T is calculated as follows:

$$T = beating\_rate \times (\frac{t^{\frac{1}{BF}}}{Max\_Iter^{\frac{1}{BF}}}) \quad (4)$$

$$beating\_rate = rand \times (\frac{PKO\_fitness(j)}{PKO\_fitness(i)}) \quad (5)$$

where, $PKO\_fitness(j)$ and $PKO\_fitness(i)$ are the fitness values of individuals j and i, and BF is a constant set to 8.

C. Diving Strategy (Exploitation Phase)

The exploitation phase, modeled on the pied kingfisher's diving behavior, is defined as:

$$X_i(t+1) = X_i(t) + HA \times o \times \alpha \times (b - X_{best}(t)) \quad (6)$$

$$HA = rand \times (\frac{PKO\_fitness(i)}{Best\_fitness}) \quad (7)$$

$$o = exp(\frac{-t}{Max\_Iter})^2 \quad (8)$$

$$b = X_i(t) + o^2 \times randn \times X_{best}(t) \quad (9)$$

where, $PKO\_fitness(i)$ denotes the fitness value of the i-th pied kingfisher, while $Best\_fitness$ represents the best fitness value obtained during the iteration process. The parameter α is a control variable calculated as $2 \times randn(1, Dim) - 1$, Where $randn$ is a uniformly distributed random number. HA and o represent the hunting abilities.

D. Co-Feeding Phase (Local Escape Phase)

This phase, inspired by the pied kingfisher's symbiosis, is defined as:

$$X_i(t+1) = \begin{cases} X_m(t) + o \times \alpha \times |X_i(t) - X_n(t)| & if\ rand > (1-PE)\ (a) \\ X_i(t) & otherwise\ \ (b) \end{cases} \quad (10)$$

$$i = 1,2,\ldots,N \quad (11)$$

$$o = exp(\frac{-t}{Max\_Iter})^2 \quad (12)$$

$$\alpha = 2 \times randn(1, Dim) - 1 \quad (13)$$

$$PE = PE_{max} - (PE_{max} - PE_{min}) \times (\frac{t}{Max\_Iter}) \quad (14)$$

where, X_m and X_n are two individuals randomly selected from the population. The predation efficiency of the pied kingfisher is denoted by PE, with fixed values $PE_{max} = 0.5$ and PE_{min}=0.

III. Dual-Layer Perturbation-Based PKO Algorithm

To enhance the robustness and global search capability of the PKO algorithm in solving complex optimization problems, this study proposes a dual-mechanism design for the evolution of its control parameters, comprising a probabilistic reverse perturbation mechanism and a heavy-tailed perturbation regulation mechanism.

These two mechanisms work synergistically to establish a control strategy characterized by jumpiness, adaptability, and nonlinear perturbations, thereby improving the algorithm's ability to escape local optima and increasing search efficiency.

A. Probabilistic Reverse Perturbation Mechanism

In the original PKO algorithm, the control parameter o evolves exponentially decreasing with respect to the iteration number t, and is expressed as follows:

$$o = exp(\frac{-t}{Max\_Iter})^2 \quad (15)$$

Although this approach can guide the algorithm to gradually transition into the fine-tuning search phase to some extent, the fixed monotonic decreasing trend tends to cause premature convergence and reduce the global search capability. To address this issue, a probabilistic reverse perturbation mechanism is introduced in this study, wherein the parameter o undergoes a reverse transformation with a certain probability during the update phase, expressed as follows:

$$o = 1 - o \quad (16)$$

The execution of this mechanism is governed by a random variable r, which is un iformly distributed between 0 and 1. When $r < p$ (where p is a predefined small probability, set to 0.1 in this study), the reverse perturbation mechanism is triggered. This design introduces an asymmetric perturbation pathway, enhancing the diversity of the search directions and thereby helping to overcome the inertia of local convergence.

B. Heavy-Tailed Perturbation Regulation Mechanism

To further enhance the adaptability of the control parameter and its ability to perform jump searches, this study introduces perturbations based on heavy-tailed distributions into the parameter o, including Lévy flight, Cauchy distribution, Student's t-distribution and Laplace distribution. Specifically, Lévy flight introduces long-distance random jumps to increase the ability of individuals to escape from the current local region; Cauchy perturbation, characterized by its extremely heavy tails, induces more aggressive search behavior, which is effective in overcoming premature convergence traps; the Student's t-distribution provides moderate-intensity asymmetric perturbations, offering good convergence stability; The Laplace distribution constructs a symmetric, centrally concentrated perturbation pattern that is beneficial for searching high-quality solutions in local neighborhoods.

The mathematical expressions of these four perturbations are given in Eq. (17)-(20).

(1) Lévy Flight Perturbation

$$o = min(1, max(0.1353, (e^{-\frac{t}{Max\_Iter}})^2 + 0.05 \times \frac{u}{|v|^{1/\beta}})) \quad (17)$$

where, t represents the current iteration number, Max_Iter denotes the maximum number of iterations, u and v are random variables drawn from the standard normal distribution, and β is the Lévy flight exponent, which is set to 1.5 in this study.

(2) Cauchy Perturbation

$$o = min(1, max(0.1353, (e^{-\frac{t}{Max\_Iter}})^2 + \sigma \times tan(\pi \times (rand - 0.5)))) \quad (18)$$

where, σ is the perturbation scale factor, set to 0.05 in this study, and $rand$ is a random number uniformly distributed between 0 and 1.

(3) Student's t-Distribution Perturbation

$$o = min(1, max(0.1353, (e^{-\frac{t}{Max\_Iter}})^2 + \sigma \times \delta_t)) \quad (19)$$

where, σ is the perturbation scale factor, set to 0.05 in this study, and δ_t is a variable following a Student's t-distribution with degrees of freedom $v = 3$.

(4) Laplace Perturbation

$$o = min(1, max(0.1353, (e^{-\frac{t}{Max\_Iter}})^2 + b \times sign(r_1 - 0.5) \times ln(1 - 2 \times |r_2 - 0.5|))) \quad (20)$$

where, b is the scale parameter of the Laplace distribution, set to 0.05 in this study, and r_1 and r_2 are random numbers uniformly distributed between 0 and 1.

Fig. 1 illustrates the variation trends of the control parameter o and its reverse transformation under different perturbation mechanisms. Fig. 1(a) shows the original control parameter o and its reverse transformation decreasing over the course of iterations. Fig. 1(b)-(e) correspond to the variations of parameter o and its reverse transformation under perturbations based on Lévy flight, Cauchy distribution, Student's t-distribution and Laplace distribution, respectively.

As observed, different perturbation mechanisms exhibit nonlinear fluctuations and jumps to varying degrees. Such perturbations not only facilitate a broader and more effective exploration of the search space in the initial stage, but also facilitate enhanced and more focused development near promising regions in subsequent iterations, thereby significantly improving the overall optimization performance.

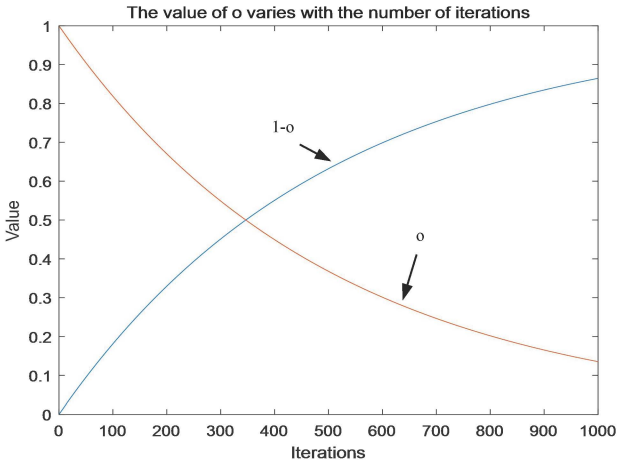

(a) Original image

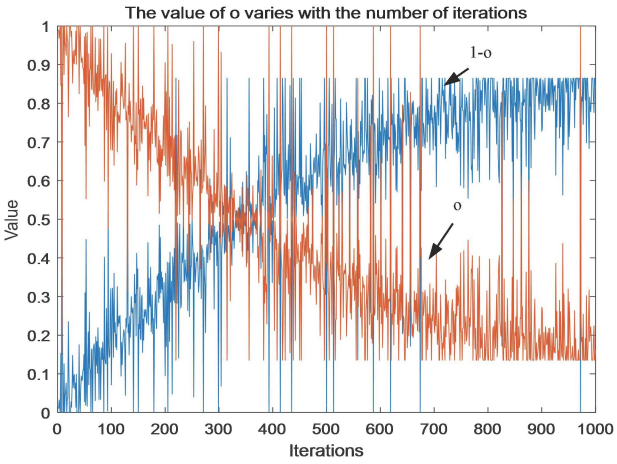

(b) Images introducing Lévy flight distribution

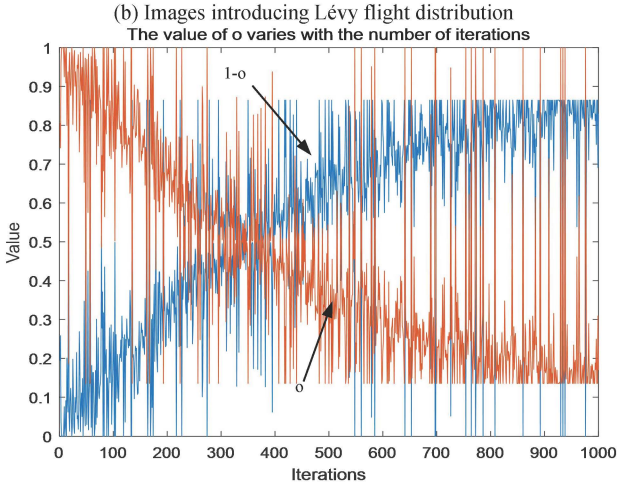

(c) Images introducing Cauchy distribution

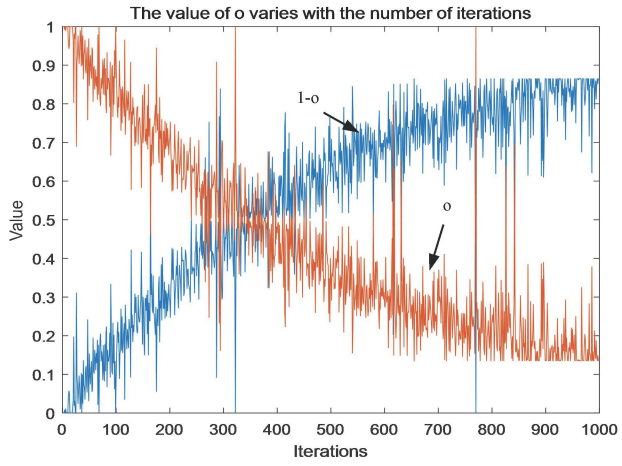

(d) Images introducing Student's t-distribution

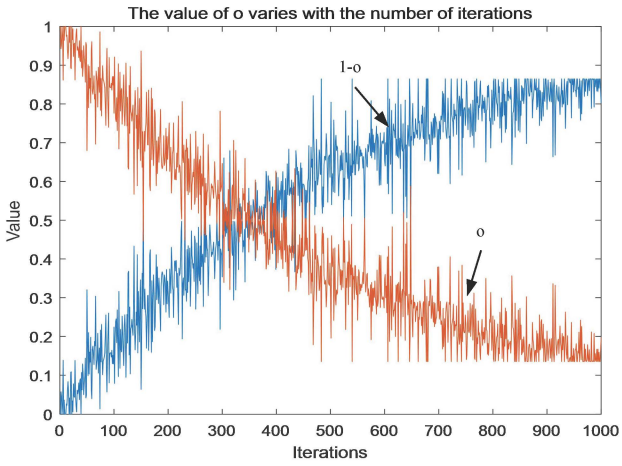

(e) Images introducing Laplace distribution

Fig. 1. The images of o and its reverse transformation under different double-layer perturbation mechanisms.

In summary, the two proposed control factor improvement mechanisms, probabilistic reverse perturbation and heavy-tailed distribution perturbation, functionally emphasize different aspects while structurally complement each other, forming a synergistic and adaptive control framework.

Specifically, the probabilistic reverse perturbation mechanism introduces a low-probability reverse operation ($o = 1 - o$) during the update of the control parameter, effectively enhancing the directional diversity and uncertainty of the search path, thereby improving the flexibility and diversity of population exploration. In contrast, the heavy-tailed perturbation mechanism dynamically regulates the evolutionary trend of the control parameter by leveraging the jumpiness and asymmetry of various typical heavy-tailed distributions such as Lévy flight, Cauchy distribution, Student's t-distribution and Laplace distribution, endowing the search behavior with stronger global jumping ability and local perturbation capacity.

From an overall algorithmic perspective, the probabilistic reverse perturbation primarily influences the directionality and uncertainty of the control parameter, whereas the heavy-tailed perturbation mainly adjusts its magnitude and dynamic responsiveness. Their collaborative effect enables the control parameter to dynamically adapt to the structure of the search space during the algorithm's execution while maintaining convergence, thus achieving a more favorable balance between exploration and exploitation.

This combined mechanism demonstrates significant performance advantages, not only enhancing the algorithm's global search capability in complex function spaces but also improving its adaptability and robustness in engineering applications. Experimental results further validate the effectiveness of this dual-perturbation strategy across various benchmark functions and practical engineering scenarios.

C. Computational Complexity Analysis

The improved algorithm introduces a dual perturbation strategy that integrates multiple heavy-tailed distributions along with a probabilistically controlled opposition-based mechanism to enhance population diversity and global search ability. Although these enhancements significantly improve the algorithm's robustness and convergence behavior, the overall computational structure remains consistent with that of the original PKO. Specifically, the additional perturbation

operations are based on basic arithmetic calculations and random sampling, which incur negligible overhead compared to the cost of objective function evaluations.The total time complexity of the improved algorithm is expressed as $O(Max\_Iter \times N \times (D + T_f))$, where Max_Iter denotes the maximum number of iterations, N is the population size, D is the dimensionality of the problem, and T_f represents the computational cost of a single objective function evaluation. The space complexity is given by $O(Max\_Iter + N \times D)$. Therefore, despite its enhanced search mechanisms, the improved algorithm maintains a computational complexity on par with the original PKO.

D. Pseudo-code of the Dual-Layer Perturbation-Based Pied Kingfisher Optimizer

Pseudo code of dual-layer perturbation-based pied kingfisher optimizer is described as follows.

```
Initialize population and algorithm parameters
Evaluate fitness of each individual
t=1
While t ≤ Max_Iter do
  For each individual Xi in the population do
    If rand() < 0.8 then
      // Exploration Phase
      If rand() > 0.5 then
        Compute T using Eq. (3)
        Update Xi using Eq. (2)
      Else
        Compute T using Eq. (5)
        Update Xi using Eq. (2)
      End if
    Else
      // Exploitation Phase
      Update Xi using Eq. (7)
    End if
    Evaluate fitness of new solution Xi
    If new fitness is better then
      Replace old solution with new Xi
    End if
  End for
  Update Best_position based on best fitness

  // Local Escape Strategy
  For each individual Xi do
    If rand() > (1 − PE) then
      Update Xi using Eq. (11a)
    Else
      Update Xi using Eq. (11b)
    End if
  End for

  Re-evaluate fitness of population
  Update Best_position if improved
  t=t+1
End While
Return Best_position, Best_fitness
```

IV. Experiment and Analysis of CEC-BC-2022 Test Function

To comprehensively validate the effectiveness of the proposed Dual-Layer Perturbation-Based Pied Kingfisher Optimizer in enhancing global search capability and convergence performance, the CEC-BC-2022 benchmark test suite was selected as the evaluation platform. This suite comprises multi-modal functions, discontinuous functions, high-dimensional rotated functions, composition functions, and hybrid functions, characterized by high complexity, strong discriminability, and considerable challenge. It is widely used for performance comparison experiments of swarm intelligence optimization algorithms. The experimental setup used 20 dimensions, a population of 30, and 1000 iterations. All algorithms ran 30 times with identical settings, and were evaluated by Best, Mean, Std, and convergence behavior. In the comparative experiments, the original PKO algorithm was used as the baseline. Subsequently, the two proposed perturbation mechanisms were incrementally incorporated to construct multiple comparative algorithm versions. The algorithm with the probability-based reverse perturbation mechanism is denoted as O-PKO; Based on this, four variants were developed by further introducing four types of heavy-tailed perturbations-Lévy flight, Cauchy distribution, Student's t-distribution and Laplace distribution-denoted as the LO-PKO, the CO-PKO, the TO-PKO and the LAO-PKO, respectively. Performance comparisons on the CEC-BC-2022 benchmarks confirm the dual-mechanism's robustness in improving global search, avoiding local optima and accelerating convergence. See Table I and Fig. 2 for results. To provide a more intuitive comparison of overall performance, a wind rose plot was generated based on the average ranking of each algorithm, as illustrated in Fig. 3. In the plot, algorithms with higher average ranks are represented by larger sectors, making it easier to visualize their relative advantages and stability across the benchmark functions.

The experimental results clearly demonstrate that the proposed dual-layer perturbation-based pied kingfisher optimizer significantly outperforms the original PKO algorithm on the CEC-2022 benchmark test suite. This fully validates the effectiveness of the proposed dual-perturbation mechanism in enhancing global search capabilities, improving the ability to escape from local optima, and accelerating convergence speed. The convergence curves reveal that all enhanced variants-starting from the O-PKO algorithm, which introduces a probability-based reverse perturbation mechanism, to LO-PKO, CO-PKO, TO-PKO and LAO-PKO, which further incorporate Lévy flight, Cauchy, Student's t- and Laplace distributions, respectively. Exhibit more rapid objective value reduction during the initial optimization phase, while maintaining improved convergence stability in the later stages.

A detailed analysis of the statistical performance further substantiates the superiority of the proposed approach. The original PKO algorithm achieved the lowest standard deviation on functions F1, F2 and F3 and produced the best solution on F6, indicating a certain degree of stability on simpler or lower-dimensional landscapes. The O-PKO variant, enhanced with the reverse perturbation mechanism, achieved the lowest standard deviation on F6, reflecting

improved exploitation capabilities. Among the heavy-tailed variants, LO-PKO attained the best mean results on F1, F2, F6, F8 and F11, and achieved the best solution on F10, exhibiting outstanding convergence precision. CO-PKO demonstrated superior average performance on F3, F9 and F10, while also generating the best results on F4, F7, F8 and F12, and the lowest standard deviations on F5, F9 and F11, showing strong overall performance and solution consistency. TO-PKO yielded optimal mean values on F7, best solutions on F1 and F3, and lowest standard deviations on F7, F8 and F10, indicating high convergence stability. LAO-PKO excelled on complex nonlinear functions by obtaining best solutions on F2, F5, F9 and F11, best mean values on F4, F5 and F12, and lowest standard deviations on F4 and F12, demonstrating its robustness in high-dimensional, non-convex problem landscapes. Finally, a comprehensive ranking based on the average performance across all benchmark functions indicates that LO-PKO achieves the best overall optimization results, followed by CO-PKO and LAO-PKO. This confirms the efficacy of integrating heavy-tailed perturbation strategies in guiding long-distance exploratory jumps and effectively avoiding premature convergence. Overall, the experimental evidence strongly supports the conclusion that the proposed dual-layer perturbation framework significantly enhances the original PKO's performance across multiple evaluation criteria, offering improved robustness, global optimization capability, faster convergence speed, enhanced solution quality, and broader practical applicability to a wide spectrum of complex real-world optimization problems.

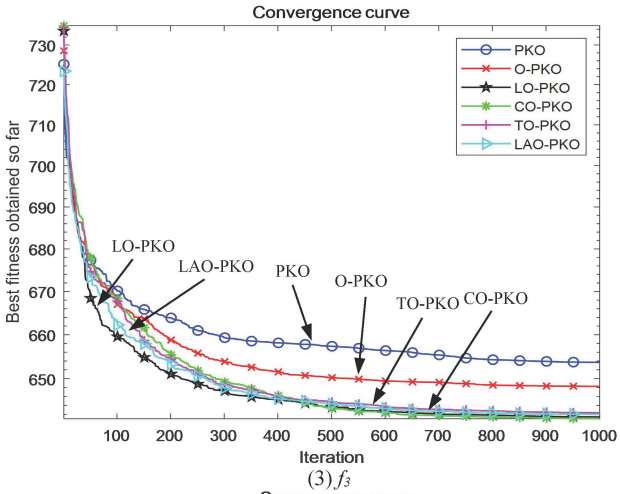

(3) f_3

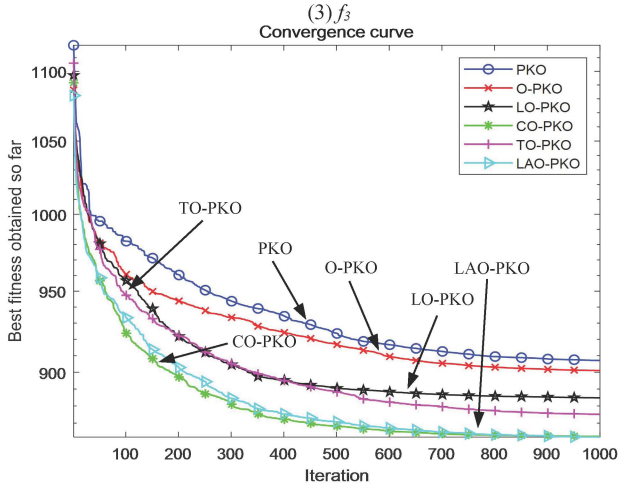

(4) f_4

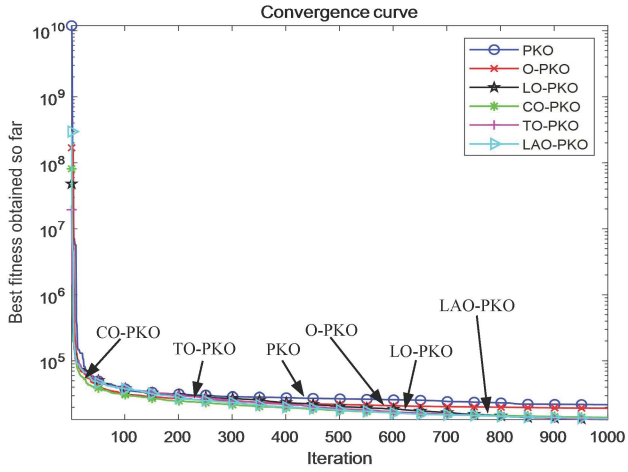

(1) f_1

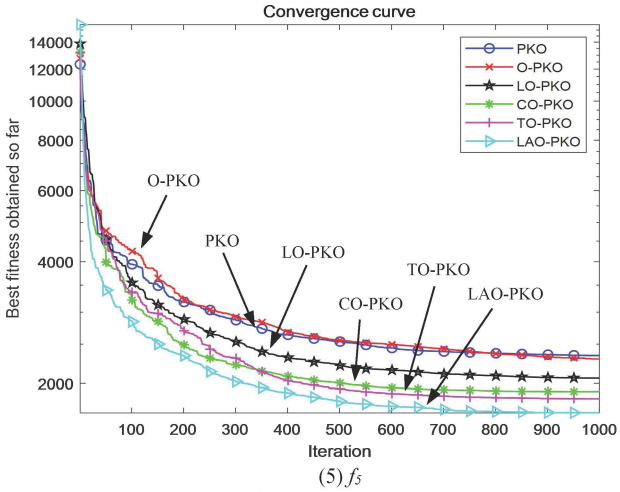

(5) f_5

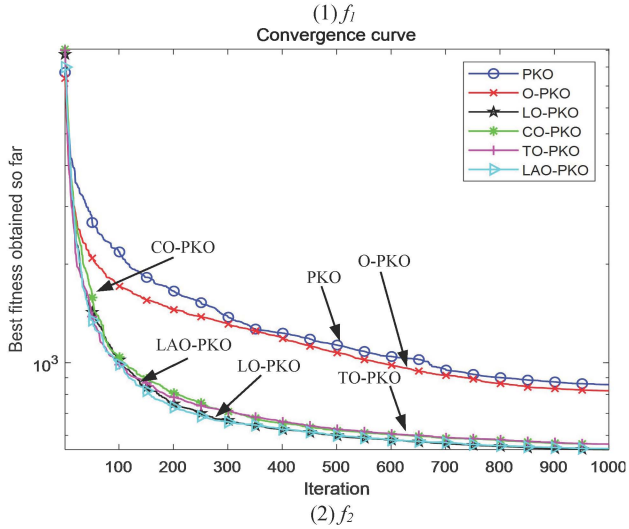

(2) f_2

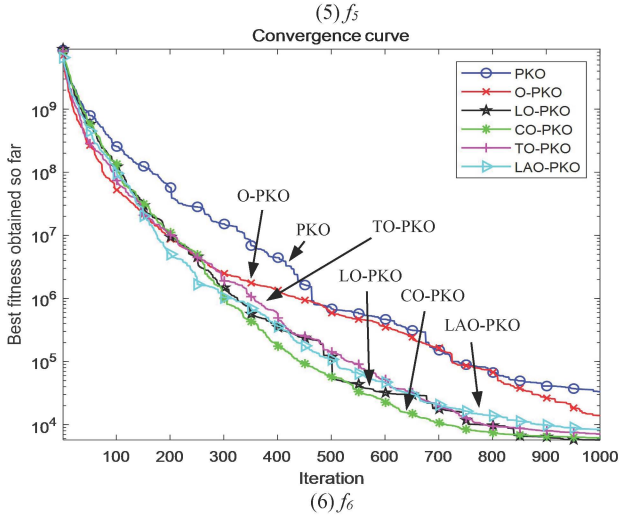

(6) f_6

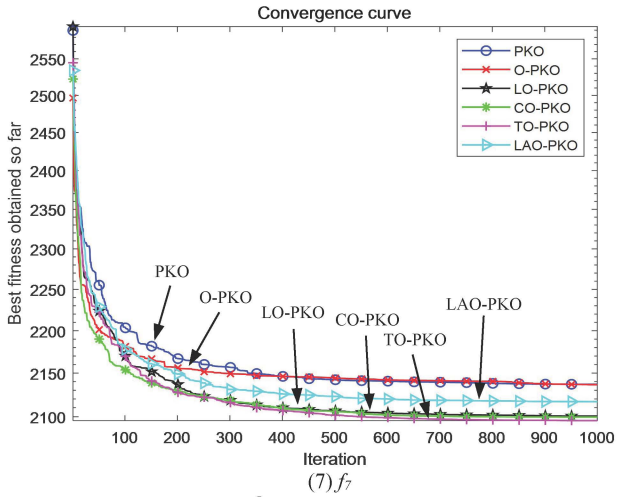

(7) f_7

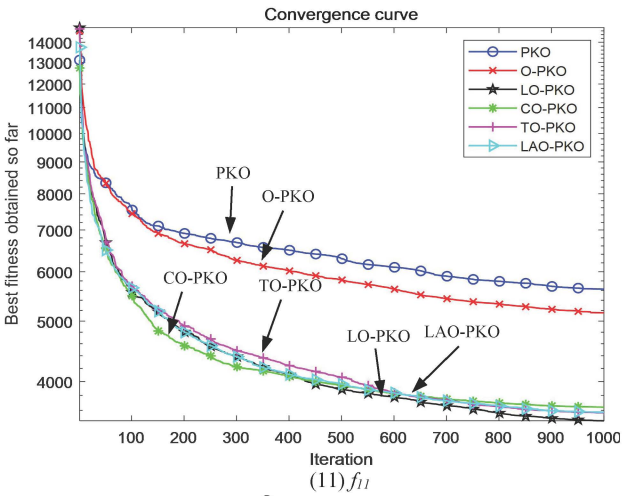

(11) f_{11}

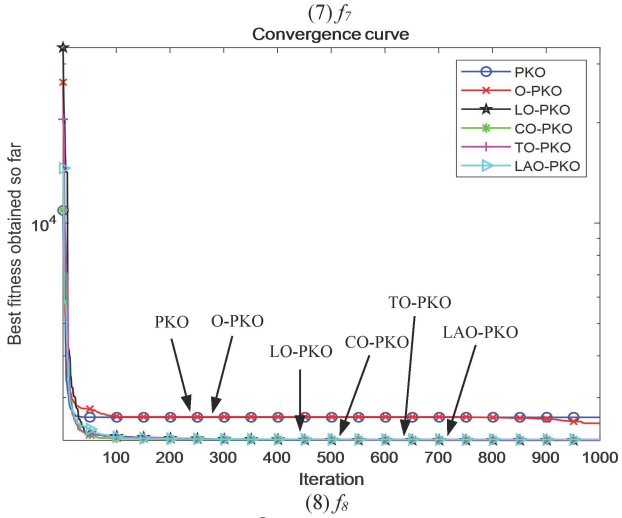

(8) f_8

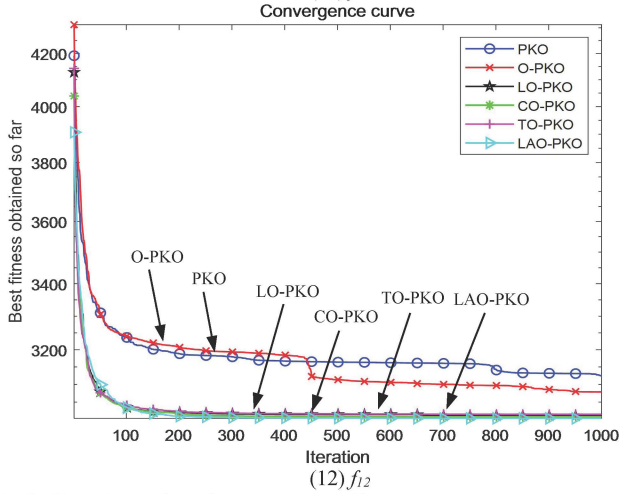

(12) f_{12}

Fig. 2. Experimental results convergence diagram.

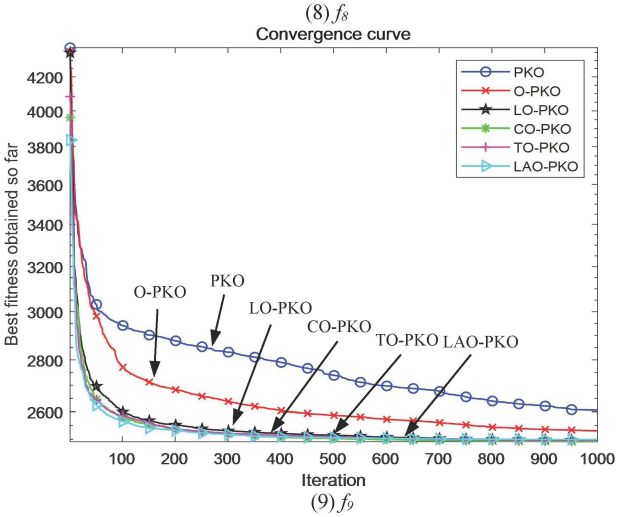

(9) f_9

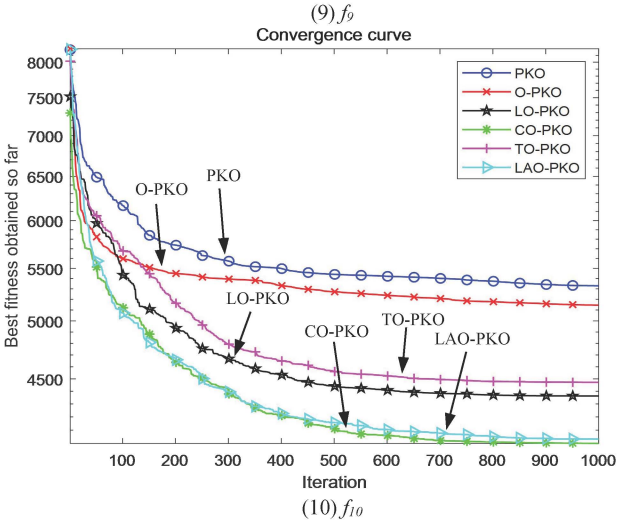

(10) f_{10}

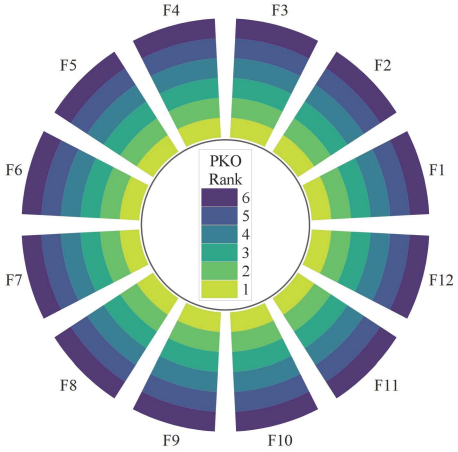

(1) PKO

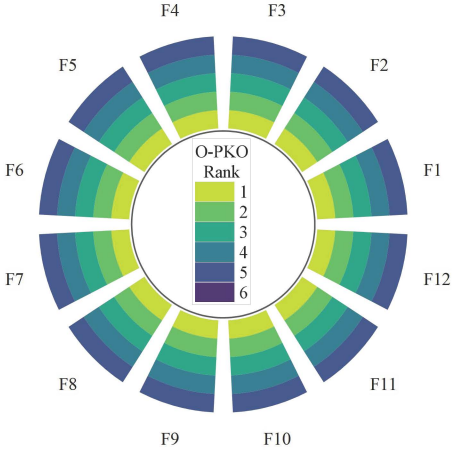

(2) O-PKO

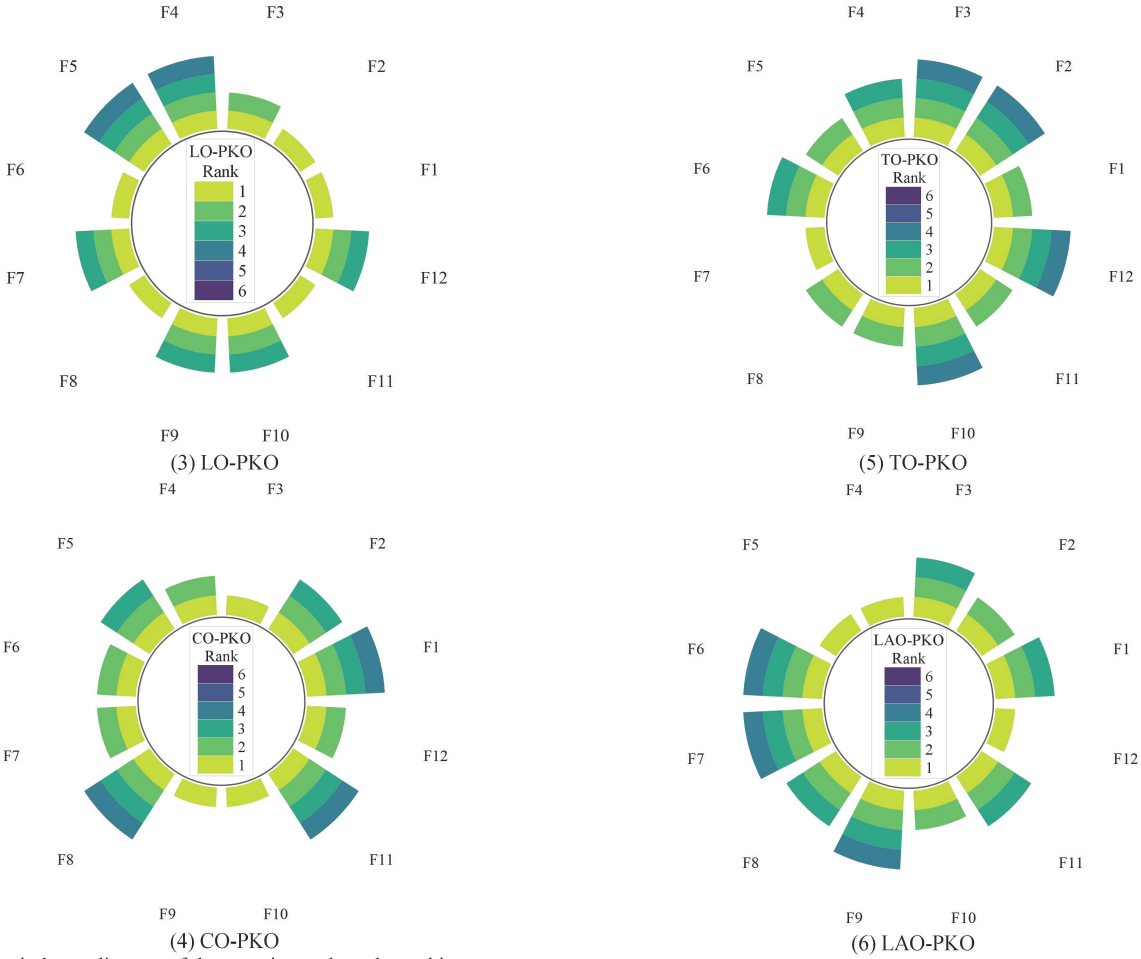

Fig. 3. The wind rose diagram of the experimental results ranking.

V. The Experiment and Analysis of Solving ELD

To further validate the applicability and effectiveness of the proposed improved algorithm in practical engineering optimization problems, this study applies the best-performing LO-PKO to the classical Economic Load Dispatch (ELD) problem. As a core optimization task in power system scheduling, the ELD problem aims to minimize the total generation cost of the system while satisfying power balance constraints and generator operating limits. The problem is characterized by nonlinearities, non-convexities, and multiple constraints. Particularly, when practical operating conditions such as valve-point effects and transmission losses are considered, higher demands are placed on the global search capability and solution accuracy of optimization algorithms. Therefore, the ELD problem is widely recognized as a standard benchmark for evaluating the engineering performance of intelligent optimization algorithms.

In the experimental design, standard power generation system models comprising 20 and 40 thermal generating units were selected as research subjects to evaluate the scalability and robustness of the proposed algorithm under different system complexities. Based on these models, the objective function was mathematically formulated as shown in Eq. (21), incorporating a quadratic fuel cost function together with valve-point effect modeling to reflect practical non-linear characteristics. Specifically, the objective function is expressed as follows:

$$MinF_i = \sum_{i=1}^{n} (\alpha_i + \beta_i P + \gamma_i P_i^2 + \left| e_i \times sin(f_i(P_i^{min} - P_i)) \right|) \quad (21)$$

where, F_i denotes the total fuel cost, and P_i represents the power output of the i-th generator. n is the total number of generating units. The constants α_i, β_i, and γ_i correspond to the fuel cost coefficients of the i-th generator. Parameters e_i and f_i represent the valve-point effect coefficients for the i -th generator, while P_i^{min} indicates the minimum permissible power output of the i-th unit. The constraints include power balance constraints, upper and lower power output limits, and permissible transmission loss modeling, which collectively ensure solution feasibility and system stability. To comprehensively evaluate the optimization capability of the LO-PKO algorithm in handling such complex real-world problems, this study compares it with the original PKO algorithm and four representative swarm intelligence optimization algorithms reported in the literature: Newton-Raphson-based Optimizer (NRBO) [14], Superb Fairy-wren Optimization Algorithm (SFOA) [15], Tuna Swarm Optimization (TSO) [16] and RRT-based Optimizer (RRTO) [17].

The selected algorithms encompass a diverse set of search strategies, including gradient-based updates, random walks, and biologically inspired behaviors, thus covering a broad spectrum of optimization paradigms. Such a comprehensive comparison enables a more robust and objective assessment of the improved algorithm generalization ability, convergence efficiency and adaptability across different types of problem landscapes.

TABLE I. DUAL-LAYER PERTURBATION-BASED PIED KINGFISHER OPTIMIZER TO OPTIMIZE THE CEC-BC-2022 FUNCTIONS

Function		PKO	O-PKO	LO-PKO	CO-PKO	TO-PKO	LAO-PKO
f_1	Best	5.6160E+03	8.2465E+03	4.5138E+03	6.0939E+03	**3.5860E+03**	4.6176E+03
	Mean	2.1890E+04	1.9351E+04	**1.3009E+04**	1.4057E+04	1.3114E+04	1.3566E+04
	Std	**1.0604E+04**	9.6022E+03	7.6726E+03	7.3631E+03	5.7568E+03	6.6400E+03
	Rank	6	5	1	4	2	3
f_2	Best	5.4484E+02	4.8723E+02	4.8252E+02	4.7476E+02	4.7805E+02	**4.6850E+02**
	Mean	8.5731E+02	8.2109E+02	**5.4274E+02**	5.6422E+02	5.6448E+02	5.4666E+02
	Std	**2.3816E+02**	3.2715E+02	4.8805E+01	6.7074E+01	5.4269E+01	6.2347E+01
	Rank	6	5	1	3	4	2
f_3	Best	6.3960E+02	6.3426E+02	6.3120E+02	6.2763E+02	**6.2629E+02**	6.3091E+02
	Mean	6.5370E+02	6.4825E+02	6.4147E+02	**6.4106E+02**	6.4240E+02	6.4206E+02
	Std	**7.2251E+00**	7.9721E+00	7.7875E+00	9.3336E+00	1.3149E+01	9.1605E+00
	Rank	6	5	2	1	4	3
f_4	Best	8.6732E+02	8.6583E+02	8.6505E+02	**8.3869E+02**	8.5397E+02	8.4713E+02
	Mean	9.0712E+02	9.0103E+02	8.8482E+02	8.6233E+02	8.7512E+02	**8.6194E+02**
	Std	2.2368E+01	2.6000E+01	1.2076E+01	1.1047E+01	1.1733E+01	**8.8623E+00**
	Rank	6	5	4	2	3	1
f_5	Best	1.5468E+03	1.9486E+03	1.5284E+03	1.6170E+03	1.1465E+03	**1.1281E+03**
	Mean	2.3420E+03	2.2964E+03	2.0598E+03	1.9073E+03	1.8325E+03	**1.6910E+03**
	Std	3.2761E+02	2.9522E+02	3.0401E+02	**1.8157E+02**	3.9608E+02	3.3706E+02
	Rank	6	5	4	3	2	1
f_6	Best	**1.9647E+03**	2.2169E+03	2.0409E+03	2.0553E+03	1.9977E+03	2.8411E+03
	Mean	3.3407E+04	1.3941E+04	**5.7209E+03**	6.1837E+03	7.1208E+03	8.4528E+03
	Std	4.8891E+04	**1.2411E+04**	3.3317E+03	4.7543E+03	5.2893E+03	5.3975E+03
	Rank	6	5	1	2	3	4
f_7	Best	2.0961E+03	2.0865E+03	2.0475E+03	**2.0363E+03**	2.0545E+03	2.0765E+03
	Mean	2.1369E+03	2.1365E+03	2.1008E+03	2.0996E+03	**2.0955E+03**	2.1169E+03
	Std	4.9553E+01	3.5900E+01	3.1678E+01	4.1339E+01	**1.8579E+01**	3.4408E+01
	Rank	6	5	3	2	1	4
f_8	Best	2.4238E+03	2.2398E+03	2.2264E+03	**2.2261E+03**	2.2291E+03	2.2267E+03
	Mean	2.6187E+03	2.5110E+03	**2.2329E+03**	2.2457E+03	2.2338E+03	2.2444E+03
	Std	1.8306E+02	2.0788E+02	6.2817E+00	3.8067E+01	**4.7736E+00**	3.8681E+01
	Rank	6	5	1	4	2	3
f_9	Best	2.4949E+03	2.4909E+03	2.4848E+03	2.4832E+03	2.4832E+03	**2.4821E+03**
	Mean	2.6060E+03	2.5303E+03	2.4965E+03	**2.4913E+03**	2.4955E+03	2.4994E+03
	Std	1.2120E+02	3.9160E+01	9.6037E+00	**6.1816E+00**	1.2011E+01	1.0695E+01
	Rank	6	5	3	1	2	4
f_{10}	Best	2.6061E+03	2.5264E+03	**2.5011E+03**	2.5024E+03	2.5032E+03	2.5019E+03
	Mean	5.3289E+03	5.1451E+03	4.3624E+03	**4.0017E+03**	4.4715E+03	4.0336E+03
	Std	1.0628E+03	1.4394E+03	1.1007E+03	1.1046E+03	**1.0547E+03**	1.1401E+03
	Rank	6	5	3	1	4	2
f_{11}	Best	3.3530E+03	3.4855E+03	3.1245E+03	3.3451E+03	3.2053E+03	**3.0774E+03**
	Mean	5.6259E+03	5.1564E+03	**3.4649E+03**	3.6401E+03	3.5694E+03	3.5761E+03
	Std	1.6888E+03	1.7136E+03	2.9642E+02	**2.4415E+02**	2.9244E+02	4.7810E+02
	Rank	6	5	1	4	2	3
f_{12}	Best	3.0074E+03	2.9829E+03	2.9751E+03	**2.9448E+03**	2.9476E+03	2.9607E+03
	Mean	3.1248E+03	3.0786E+03	3.0119E+03	3.0092E+03	3.0158E+03	**3.0046E+03**
	Std	1.0710E+02	1.1296E+02	3.4191E+01	4.1288E+01	4.8768E+01	**2.9103E+01**
	Rank	6	5	3	2	4	1
Friedman		6	5	2.25	2.42	2.75	2.58
Rank		6	5	1	2	4	3

A. Case1: 20 Unit

In Case 1, the total load demand was set at 2500 MW, with the optimization conducted over 1000 iterations using a population size of 20 and problem dimension of 20. To ensure statistical reliability, all algorithms were independently executed 30 times under identical parameter settings. Performance indicators such as best solution, mean value, standard deviation, and convergence speed were systematically recorded. Detailed algorithmic parameters and system-specific generation constraints, including fuel cost coefficients, are provided in Tables II and III, respectively.

The summarized results for the 20-unit system across different algorithms are presented in Table IV, with corresponding convergence profiles shown in Fig. 4. Furthermore, a racing plot is illustrated in Fig. 5 to visually compare the total generation costs achieved by different algorithms.

In this plot, each algorithm is assigned a track lane and its position along the track reflects its corresponding cost performance. Algorithms with lower total costs are positioned farther from the starting line and closer to the front, indicating superior economic efficiency. This reverse-mapping design provides a clear and intuitive understanding of the comparative cost effectiveness of each method.

The simulation outcomes reveal that the proposed LO-PKO algorithm attains superior overall performance in solving the 20-unit Economic Load Dispatch (ELD) problem. Specifically, LO-PKO achieves an active power loss (PL) of 71.56 MW and a total delivered power (PD) of 2571.58 MW, accurately satisfying the system's power balance constraints, including transmission losses.

Notably, LO-PKO obtains the lowest total fuel cost of \$61,870.75, surpassing the original PKO algorithm (\$61,896.93) as well as other advanced meta-heuristics including NRBO (\$61,944.24), SFOA (\$62,108.18), TSO (\$61,873.64) and RRTO (\$61,892.01). Although TSO yields a comparable fuel cost, LO-PKO demonstrates a more balanced and efficient power allocation scheme.

A detailed examination of power distribution shows that SFOA and RRTO report relatively lower transmission losses (63.50 MW and 67.23 MW, respectively), resulting in a correspondingly lower total generated power (PD). This deviation may indicate potential imbalances between supply and demand, thereby raising concerns about system reliability. Conversely, NRBO more precisely meets the total power delivery requirements (PD = 2570.63 MW) but at the expense of higher fuel costs, reflecting limited optimization efficiency.

The original PKO and TSO algorithms produce intermediate results in both power loss and cost metrics but fall short of matching the enhanced convergence stability and overall effectiveness of LO-PKO.

Overall, the experimental analysis confirms the enhanced adaptability, convergence speed, and robustness of the LO-PKO algorithm in addressing the nonlinear, constrained nature of the ELD problem, validating its potential for practical deployment in power system economic dispatch applications.

TABLE II. PARAMETER SETTINGS OF EACH ALGORITHM

Algorithm	Main parameters setting
PKO	*BF=8;PEmax=0.5;PEmin=0;*
LO-PKO	*BF=8;PEmax=0.5;PEmin=0;*
NRBO	*DF=0.6;Flag=1;*
SFOA	*C=0.8;T=0.5;*
TSO	*aa=0.7;z=0.05;*
RRTO	*C=10;*

TABLE III. THE FUEL COST COEFFICIENT AND POWER GENERATION LIMIT OF 20 GENERATING UNITS

Unit	α_i	β_i	γ_i	P_{min}	P_{max}
1	1000	18.19	0.00068	150	600
2	970	19.26	0.00071	50	200
3	600	19.80	0.00650	50	200
4	700	19.10	0.00500	50	200
5	420	18.10	0.00738	50	160
6	360	19.26	0.00612	20	100
7	490	17.14	0.00790	25	125
8	660	18.92	0.00813	50	150
9	765	18.27	0.00522	50	200
10	770	18.92	0.00573	30	150
11	800	16.69	0.00480	100	300
12	970	16.76	0.00310	150	500
13	900	17.36	0.00850	40	160
14	700	18.70	0.00511	20	130
15	450	18.70	0.00398	25	185
16	370	14.26	0.07120	20	80
17	480	19.14	0.00890	30	85
18	680	18.92	0.00713	30	120
19	700	18.47	0.00622	40	120
20	850	19.79	0.00773	30	100

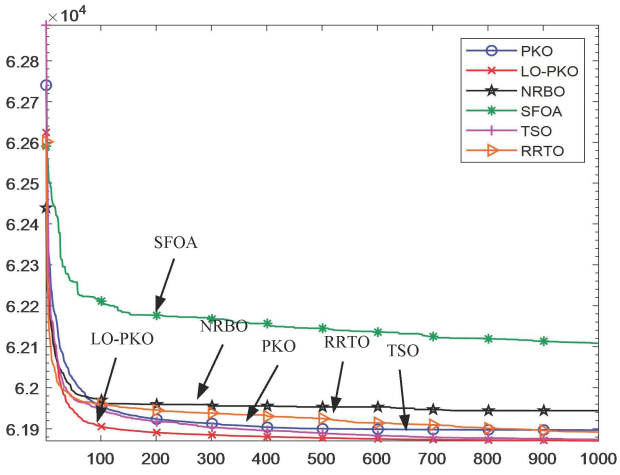

Fig. 4. Experimental convergence diagram of 20 unit.

B. Case2: 40 Unit

To further assess the scalability and practical applicability of the proposed LO-PKO, we conducted comprehensive experiments on a large-scale Economic Load Dispatch (ELD) problem comprising 40 generating units. In this scenario, the total load demand was set at 10,500 MW, with a problem dimension of 40 and a population size fixed at 50. The maximum number of iterations was limited to 1000. To ensure the statistical significance and robustness of the results, all algorithms were independently executed 30 times. Key performance indicators, including best solution, mean value, standard deviation, and convergence characteristics, were systematically recorded for in-depth comparative analysis. The detailed fuel cost coefficients and generation constraints for the 40-unit system are provided in Table V. Simulation outcomes generated by various algorithms under these settings are summarized in Table VI, with corresponding convergence curves depicted in Fig. 6. The racing plot based on the total cost is shown in Fig. 7.

The experimental results clearly indicate that the proposed LO-PKO algorithm delivers superior performance in solving the large-scale 40-unit ELD problem. Specifically, under the power demand constraint of 10,500 MW, LO-PKO attains the lowest total fuel cost of $121,556.86, achieving a notable cost reduction of approximately 2.23% compared to the original PKO algorithm, which incurred a total cost of $124,326.98.

TABLE IV. COMPARISON OF EXPERIMENTAL RESULTS OF UNIT 20

Unit	PKO	LO-PKO	NRBO	SFOA	TSO	RRTO
P_1	511.02	529.89	531.97	247.92	517.18	499.24
P_2	108.45	133.95	138.77	182.51	145.87	179.45
P_3	114.91	76.14	93.74	149.66	89.45	109.51
P_4	97.23	85.30	115.87	191.99	99.62	52.79
P_5	142.69	117.38	93.86	105.41	118.06	80.26
P_6	72.56	82.43	59.29	33.33	48.20	49.39
P_7	119.14	83.07	68.03	54.93	104.07	101.16
P_8	80.87	71.10	99.76	113.97	86.65	99.75
P_9	81.10	142.30	56.79	93.47	105.34	154.95
P_{10}	75.29	117.70	35.25	49.27	101.77	146.84
P_{11}	217.18	188.93	237.77	265.02	189.31	196.50
P_{12}	334.68	338.83	286.53	306.62	329.83	277.05
P_{13}	90.56	88.73	148.85	159.57	97.89	122.40
P_{14}	47.59	82.42	126.73	118.28	94.43	56.78
P_{15}	115.40	138.73	95.46	130.45	134.48	173.18
P_{16}	62.00	39.80	44.84	20	49.90	40.93
P_{17}	45.67	54.44	82.85	84.96	31.91	41.36
P_{18}	89.71	70.47	104.50	63.80	82.26	73.72
P_{19}	105.51	83.21	94.08	103.61	81.78	60.11
P_{20}	58.59	46.77	55.67	88.78	62.61	51.86
P_L	70.12	71.56	70.63	63.50	69.80	67.23
P_D	2570.12	2571.58	2570.63	2563.56	2570.11	2567.25
Cost	61896.93	61870.75	61944.24	62108.18	61873.64	61892.01

TABLE V. THE FUEL COST COEFFICIENT AND POWER GENERATION LIMIT OF 40 GENERATING UNITS

Unit	α_i	β_i	γ_i	e_i	f_i	P_{min}	P_{max}
1	94.705	6.73	0.0069	100	0.084	36	114
2	94.705	6.73	0.0069	100	0.084	36	114
3	309.54	7.07	0.02028	100	0.084	60	120
4	369.03	8.18	0.00942	150	0.063	80	190
5	148.89	5.35	0.0114	120	0.077	47	97
6	222.33	8.05	0.01142	100	0.084	68	140
7	267.71	8.03	0.00357	200	0.042	110	300
8	391.98	6.99	0.00492	200	0.042	135	300
9	455.76	6.60	0.00573	200	0.042	135	300
10	722.82	12.9	0.00605	200	0.042	130	300
11	635.2	12.9	0.00515	200	0.042	94	375
12	654.69	12.8	0.00569	200	0.042	94	375
13	913.4	12.5	0.00421	300	0.035	125	500
14	1760.4	8.84	0.00752	300	0.035	125	500
15	1728.3	9.15	0.00708	300	0.035	125	500
16	1726.3	9.15	0.00708	300	0.035	125	500
17	647.85	7.97	0.00313	300	0.035	220	500
18	649.69	7.95	0.00313	300	0.035	220	500
19	647.83	7.97	0.00313	300	0.035	242	550
20	647.81	7.97	0.00313	300	0.035	242	550
21	785.96	6.63	0.00298	300	0.035	254	550
22	785.96	6.63	0.00298	300	0.035	254	550
23	794.53	6.66	0.00284	300	0.035	254	550
24	794.53	6.66	0.00284	3o0	0.035	254	550
25	801.32	7.10	0.00277	300	0.035	254	550
26	801.32	7.10	0.00277	300	0.035	254	550
27	1055.1	3.33	0.52124	120	0.077	10	150
28	1055.1	3.33	0.52124	120	0.077	10	150
29	1055.1	3.33	0.52124	120	0.077	10	150
30	148.89	5.35	0.01140	120	0.077	47	97
31	222.92	6.43	0.00160	150	0.063	60	190
32	222.92	6.43	0.00160	150	0.063	60	190
33	222.92	6.43	0.00160	150	0.063	60	190
34	107.87	8.95	0.0001	200	0.042	90	200
35	116.58	8.62	0.0001	200	0.042	90	200
36	116.58	8.62	0.0001	200	0.042	90	200
37	307.45	5.88	0.0161	80	0.098	25	110
38	307.45	5.88	0.0161	80	0.098	25	110
39	307.45	5.88	0.0161	80	0.098	25	110
40	647.83	7.97	0.00313	300	0.035	242	550

In addition, LO-PKO surpasses other leading meta-heuristic algorithms, including NRBO ($123,832.70), SFOA ($146,290.73), TSO ($123,313.18) and RRTO ($125,827.80), highlighting its superior cost-efficiency and optimization capability in large-scale, nonlinear constrained problems. The pronounced cost advantage and consistent convergence performance of LO-PKO reflect its enhanced ability to effectively navigate complex solution spaces.

TABLE VI. COMPARISON OF EXPERIMENTAL RESULTS OF UNIT 40

Unit	PKO	LO-PKO	NRBO	SFOA	TSO	RRTO
P_1	81.23	111.16	103.28	114	52.16	113.51
P_2	54.11	36	44.04	114	105.40	114
P_3	109.08	117.06	101.32	120	117.16	118.31
P_4	190.00	185.04	181.63	190	156.69	188.31
P_5	84.38	94.66	94.06	97	87.41	95.84
P_6	126.40	136.26	131.28	68	121.54	121.31
P_7	297.15	292.08	241.19	300	254.92	297.52
P_8	297.96	292.96	298.47	300	223.95	300
P_9	297.95	292.10	288.96	135	255.64	298.30
P_{10}	294.16	156.03	269.33	300	206.83	296.24
P_{11}	242.08	138.11	330.97	375	128.07	365.88
P_{12}	361.91	94	338.42	375	94.12	286.41
P_{13}	383.37	125	198.97	500	365.15	415.06
P_{14}	455.64	125	215.08	500	477.09	426.44
P_{15}	324.13	486.84	487.25	125	307.77	417.30
P_{16}	388.57	487.54	456.95	500	486.61	403.63
P_{17}	354.70	486.78	264.14	500	499.68	419.01
P_{18}	280.81	500	489.46	500	499.96	411.13
P_{19}	549.07	550	535.78	550	459.93	418.67
P_{20}	547.79	472.33	529.05	550	506.86	442.17
P_{21}	453.72	535.49	549.37	254	505.17	364.07
P_{22}	503.11	530.07	550	254	536.62	456.29
P_{23}	550.00	531.99	495.30	550	376.33	451.47
P_{24}	463.43	536.37	491.31	254	504.49	516.57
P_{25}	281.83	522.25	526.07	550	518.15	420.05
P_{26}	542.56	535.59	549.99	550	514.37	382.51
P_{27}	35.63	10	20.51	10	10.09	15.31
P_{28}	56.52	14.72	21.46	10	13.95	30.85
P_{29}	37.93	10	18.89	10	16.19	18.49
P_{30}	64.22	94.42	86.33	97	89.69	94.39
P_{31}	169.04	184.98	121.67	190	189.97	162.05
P_{32}	124.52	190	179.03	60	189.89	182.16
P_{33}	189.99	183.46	189.99	60	181.23	186.30
P_{34}	191.11	200	190.01	119.03	194.07	147.17
P_{35}	199.99	194.74	130.06	142.24	177.22	200
P_{36}	165.00	194.74	103.12	200	200.00	200
P_{37}	30.10	107.08	36.72	74.56	110.00	92.71
P_{38}	93.71	102.46	105.89	25	109.74	108.77
P_{39}	77.17	107.14	31.65	25	105.37	108.82
P_{40}	550.00	535.59	503.00	550	549.94	414.65
P_D	1.05E+04	1.05E+04	1.05E+04	1.02E+04	1.05E+04	1.05E+04
$Cost$	124326.98	121556.86	123832.70	146290.73	123313.18	125827.80

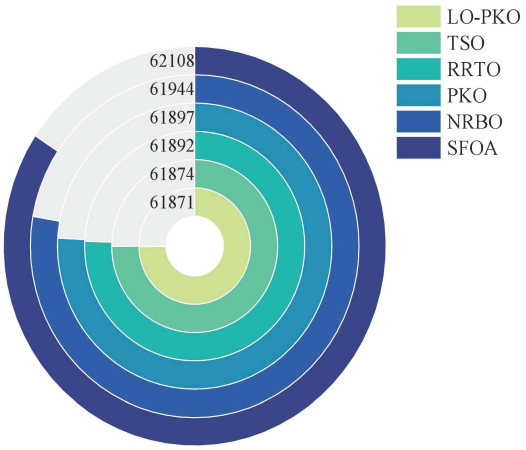

Fig. 5. The total cost of 20 units racing plot.

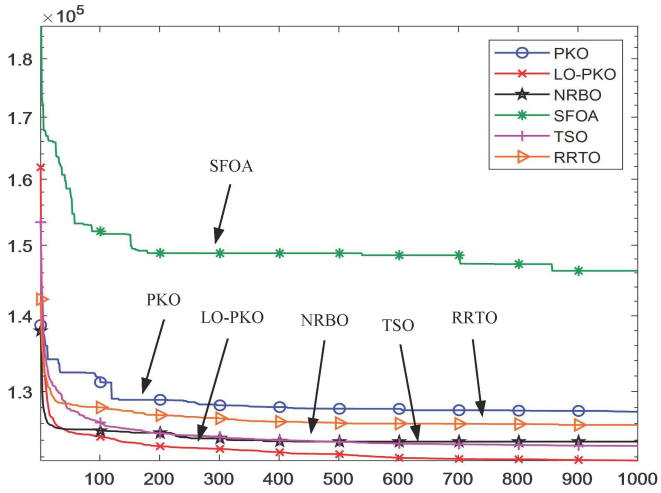

Fig. 6. Experimental convergence diagram of 40 unit.

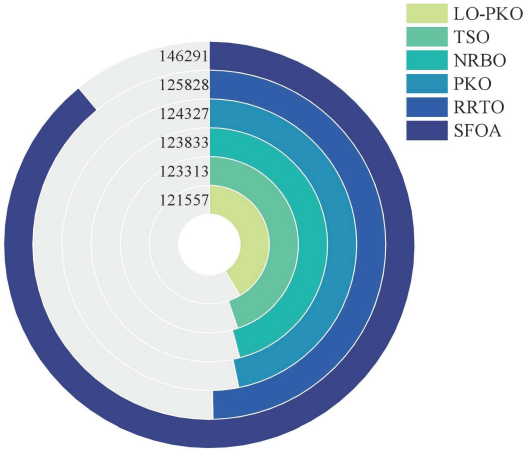

Fig. 7. The total cost of 40 units racing plot.

This substantial improvement is primarily attributed to the dual-layer perturbation mechanisms integrated within LO-PKO, which proficiently balance global exploration and local exploitation. Such a balance enables the algorithm to avoid premature convergence to local optima while maintaining stable convergence rates, thereby ensuring feasible and near-optimal solutions under multiple constraints. Consequently, the LO-PKO algorithm demonstrates strong potential for practical deployment in large-scale power system economic dispatch tasks requiring high reliability and efficiency.

VI. CONCLUSION

This paper proposes an enhanced meta-heuristic algorithm, the dual-layer perturbation-based Pied Kingfisher Optimizer, to address the limitations of the original Pied Kingfisher Optimizer (PKO), specifically its tendency toward premature convergence and limited local search capability when dealing with complex optimization problems. The dual-layer perturbation-based Pied Kingfisher Optimizer retains the foundational structure of PKO while introducing a probability-controlled reverse perturbation mechanism to enhance population diversity. Furthermore, it incorporates a suite of heavy-tailed distributions, including Lévy flight, Cauchy distribution, Student's t-distribution and Laplace distribution, to strengthen the algorithm's ability to escape local optima and strike a balance between global exploration and local exploitation.

To comprehensively evaluate the performance of the proposed algorithm, extensive experiments were conducted on the CEC-BC-2022 benchmark function suite. Compared with the original PKO and other perturbation-based variants, the LO-PKO algorithm demonstrates not only faster convergence speed but also higher convergence accuracy. Among all the tested variants, LO-PKO achieves the best overall performance, thereby validating the effectiveness of the dual-layer perturbation mechanism in enhancing optimization outcomes.

Beyond benchmark testing, the practical applicability of Dual-Layer Perturbation-Based Pied Kingfisher Optimizer was further evaluated on real-world engineering problems. The algorithm was applied to solve both 20-unit and 40-unit Economic Load Dispatch (ELD) problems, classic constrained nonlinear optimization tasks in power system scheduling. Simulation results indicate that LO-PKO not only satisfies complex operational constraints (e.g., power balance, generation limits, and valve-point effects), but also achieves the lowest total fuel cost among all compared algorithms, including PKO, NRBO, SFOA, TSO and RRTO. Notably, in the 40-unit ELD scenario with a total power demand of 10,500 MW, LO-PKO attained a minimum fuel cost of $121,556.86, reducing the cost by 2.23% compared to the original PKO and outperforming all other competitors. These results underscore LO-PKO's robustness, scalability, and suitability for large-scale, high-dimensional engineering optimization tasks.

In conclusion, the proposed Dual-Layer Perturbation-Based PKO algorithm exhibits outstanding performance across both theoretical benchmarks and practical applications. Its strong convergence capability, adaptability to real-world constraints, and consistent optimization quality highlight its generalization and potential for widespread adoption. Future work will focus on extending dual-layer perturbation-based Pied Kingfisher Optimizer to address multi-objective optimization, dynamic environment adaptation and large-scale high-dimensional problems, further enhancing its utility in intelligent decision-making and resource allocation systems in complex engineering domains.

REFERENCES

[1] R. Priyadarshi, and R. R. Kumar. "Evolution of Swarm Intelligence: A Systematic Review of Particle Swarm and Ant Colony Optimization Approaches in Modern Research," *Archives of Computational Methods in Engineering*, pp. 1-42, 2025.

[2] E. Dada, S. Joseph, and D. Oyewola. "Application of Grey Wolf Optimization Algorithm: Recent Trends, Issues, and Possible Horizons", *Gazi University Journal of Science*, vol. 35, no. 2, pp. 485-504, 2022.

[3] Y. Shen, J. Wu, M. Ma, X. Du, and D. Niu. "Application of an Improved Differential Evolution Algorithm in Practical Engineering," *Concurrency and Computation: Practice and Experience*, vol. 37, no. 3, pp. e8358, 2025.

[4] S. Lin, J. Wang, B. Huang, X. Kong, and H. Yang. "Bio Particle Swarm Optimization and Reinforcement Learning Algorithm for Path Planning of Automated Guided Vehicles in Dynamic Industrial Environments," *Scientific Reports*, vol. 15, pp. 463, 2025.

[5] H. D. Nguyen, and L. H. Pham. "Determining Solutions to New Economic Load Dispatch Problems by War Strategy Optimization Algorithm," *International Journal of Renewable Energy Development*, vol. 14, no. 1, pp. 124-135, 2025.

[6] A. Babiker, S. S. Ahmad, I. Ahmed, M. Khalid, M. A. Abido, and F. S. Al-Ismail. "Optimal Power Flow: A Review of State-of-the-Art Techniques and Future Perspectives," *IEEE Access*, vol. 13, pp. 60012-60039, 2025

[7] A. Prapanca, N. Belhaouas, and I. Mahmoud. "Modified FATA Morgana Algorithm Based on Levy Flight," *Vokasi Unesa Bulletin of Engineering, Technology and Applied Science*, vol. 2, no. 1, pp. 1-11, 2025.

[8] S. Liu, H. Shen, H. Che, B. Wang, C. Wang, C. Zhang, G. Shao, S. Feng, H. Wang, and K. Wang. "Inversion of Rayleigh Wave Dispersion Curves Integrating the Osprey-Cauchy and Pigeon-inspired Optimization Algorithm," *Acta Geophysica*, vol. 73, pp. 3195-3212, 2025.

[9] J. L. Kirkby, D. H. Nguyen, and D. Nguyen. "Moments of Student's t-distribution: A Unified Approach", *Modern Stochastics: Theory and Applications*, pp. 1-13, 2025.

[10] V. Jilesh, and A. Pournami. "On a Generalization of Laplace Distribution with Applications," *International Journal of Data Science and Analytics*, pp. 1-102, 2025.

[11] M. Bee. "A Parsimonious Dynamic Mixture for Heavy-tailed Distributions," *Mathematics and Computers in Simulation*, vol. 230, pp. 193-206, 2025.

[12] BouaoudaAnas, A. Hashimfatma, SayoutiYassine, and G. Hussienabdelazim. "Pied Kingfisher Optimizer: A New Bio-inspired Algorithm for Solving Numerical Optimization and Industrial Engineering Problems," *Neural Computing and Applications*, vol. 36, pp. 15455-15513, 2025.

[13] S. Janefar, P. Chowdhury, R. Yeassin, M. Hasan, and N. U. R. Chowdhury. "Comparative Performance Evaluation of Economic Load Dispatch Using Metaheuristic Techniques: A Practical Case Study for Bangladesh," *Results in Engineering*, vol. 26, pp. 104720, 2025.

[14] R. Sowmya, M. Premkumar, and P. Jangir. "Newton-Raphson-based Optimizer: A New Population-based Metaheuristic Algorithm for Continuous Optimization Problems," *Engineering Applications of Artificial Intelligence*, vol. 128, pp. 107532, 2024.

[15] H. Jia, X. Zhou, J. Zhang, and S. Mirjalili. "Superb Fairy-wren Optimization Algorithm: A Novel Metaheuristic Algorithm for Solving Feature Selection Problems," *Cluster Computing*, vol. 28, pp. 246, 2025.

[16] L. Xie, T. Han, H. Zhou, Z. R. Zhang, B. Han, and A. Tang. "Tuna Swarm Optimization: A Novel Swarm-Based Metaheuristic Algorithm for Global Optimization," *Computational Intelligence and Neuroscience*, vol. 1, pp. 9210050, 2021.

[17] L. G. Jin, L. Tao, and S. B. Jun. "RRT-Based Optimizer: A Novel Metaheuristic Algorithm Based on Rapidly-Exploring Random Trees Algorithm," *IEEE Access*, vol. 13, pp.42744-42776, 2025.